# Look-ahead Decision Making for Renewable Energy: A Dynamic "Predict and Store" Approach

Jingxing Wang, Seokhyun Chung, Abdullah AlShelahi, Raed Kontar, Eunshin Byon, Romesh Saigal\*<sup>†</sup>

October 2, 2021

#### Abstract

This paper presents an integrative methodology for managing and stabilizing the output of a wind/solar farm using storage devices in a cost effective and real-time manner. We consider the problem where a renewable farm should decide the amount of energy charged into or withdrawn from the battery given the stochasticity and time varying nature in the renewable energy power output. Our methodology features a seamless integration of a non-myopic decision framework and a sequential non-parametric predictive model based on functional principal component analysis. A key feature of our algorithm is that it quantifies costs over a rolling horizon where both predictions and decisions are updated on the fly as new data is acquired. Our technology is tested on the California ISO dataset. The case study provides a proof-of-concept that highlights both the benefits and ease of implementation of our forward looking framework.

Keywords: Renewable energy, Battery storage, Look-ahead optimization, Joint prediction and prescription, Functional principal component analysis, Bayesian inference.

### 1 Introduction

Recently there has been considerable emphasis on replacing the generation of electric energy from fuel-based conventional sources with renewable sources like solar and wind [1]. The integration of renewable energy into the grid system provides an environmentally friendly solution to reduce carbon emission from conventional power generation. Many states in the U.S. have set goals of achieving such a switch, and these are being consistently updated. Texas recorded 26,045 MW of electric energy generated by renewal sources in 2017, beating

<sup>\*</sup>J. Wang, S. Chung, A. AlShelahi, R. Kontar, E. Byon, and R. Saigal are with the Department of Industrial & Operations Engineering, University of Michigan, Ann Arbor, MI 48109, USA e-mail: (jef-fwjx@umich.edu; seokhc@umich.edu; Shelahi@umich.edu; alkontar@umich.edu; ebyon@umich.edu; rsai-gal@umich.edu)

<sup>&</sup>lt;sup>†</sup>This work was supported in part by the U.S. National Science Foundation uder Grants IIS-1741166 and ECCS-1709094. (*Corresponding author: Raed Kontar*)

its goal for 2025 by 250% [2]. California has set the goal of 100% by 2045 up from 50% by 2030, Massachusetts has set 55% by 2050, New Jersey has set 50% by 2030, etc [2]. Renewable energy will continue to play an important role in electricity production in the future. Similar trends have been observed in other countries [3].

The most common sources of renewable energy are wind and solar. Despite being attractive due to their low carbon imprint and relatively low production costs, the power output from these systems is highly volatile as it depends on the uncontrollable and time-varying weather conditions. To cope with such volatility, grid operators often rely on expensive ancillary services, negating some of the attractiveness of the renewables [4,5].

In addition, the solar and wind power outputs have diurnal patterns. For example, solar output is available only during the day time. Current statistics show that on a yearly basis, more than 30% of the electricity load in California is met by wind and solar power, while during certain days, the renewable energy can contribute to over 50% of the demand during the day time, but less than 20% in the evening and night [6]. The diurnal pattern in California is called a "duck curve", where the net load, i.e., the total electricity demand minus the solar plus wind energy generation, is characterized by the duck shaped curve, as shown in Figure 1 [7]. To highlight the problem, at around 2pm the solar plants produce the large amount of energy for the day, so the net load is small. However, the sun sets and the solar energy output quickly drops to zero at around 6pm in the evening. At the same time, consumers increase the demand by turning on their lights and air conditioners and the total load rises dramatically.

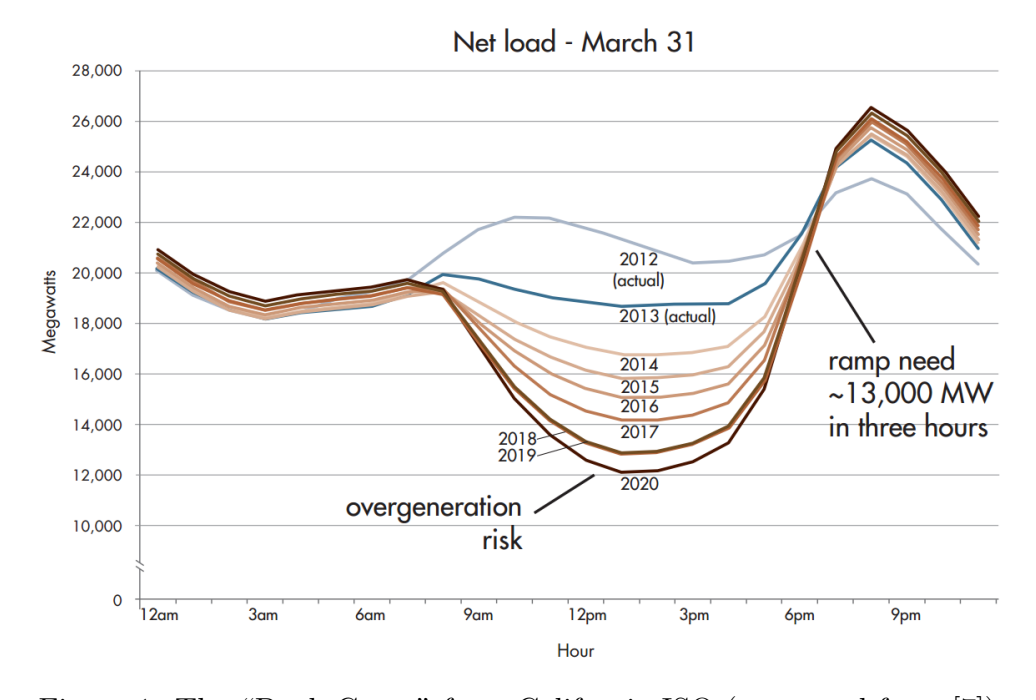


Figure 1: The "Duck Curve" from California ISO (excerpted from [7])

The steep ramp up in the "duck curve" is accommodated by conventional power plants. Because conventional plants have a limited ramping up rate, the California ISO operates them at low levels. During noon, their low level production together with the renewable energy exceeds the amount of total load. As a result, the California ISO often curtails

part of renewable energy generated and frequently observes curtailment of 20 to 30 percent of the solar capacity [8]. The excess conventional plant operations and renewable energy curtailment raise the cost of power grid operations, thus significantly decreasing its economic value [9]. To address these challenges, grid operators increasingly rely on storage devices, including pumped hydro, battery, and flywheels [10, 11]. For example, battery technology is being used to stabilize the output in micro grids and even nationwide grids [10]. Tesla's 100MW/129MWh Powerpack project in South Australia was also tested specifically for this purpose [11].

In this paper, we propose a look-ahead dynamic optimization model to manage the variability and intermittency problems in renewable sources through using battery devices. Our approach is data-driven and exploits historical data to decide how much energy needs to be stored to, or withdrawn from, energy storage devices, as well as the purchase decisions from the electricity spot market.

Such short-term decisions are typically made at each hour (or at a shorter duration, e.g., every 5 minutes), after the commitment levels from renewables are decided on the day-ahead energy market. Although our focus is to optimize short-term battery operations, we do so via a look-ahead framework which utilizes future renewable energy pattern predictions. This distinguishes this work from the myopic approach which optimizes a "snap-shot" operation of the system at each decision point, without taking the future renewable generation into consideration.

Specifically, optimal storage and energy purchase decisions are formulated as a convex dynamic programming (DP) which minimizes costs over future steps in reference to the expected total purchase and salvage costs for the grid entities. Using historical data we then provide a non-parametric forecasting model, based on functional principal component analysis (FPCA), that predicts the future trajectory of renewable supply whenever new data is obtained. A salient aspect of FPCA is that, despite its non-parametricity, it features a linear decomposition of the longitudinal signals which in turn facilitates efficient model updating using an empirical Bayes procedure. Given the FPCA model, our framework updates predictions of the future trajectory of renewable supply whenever new data is obtained and iteratively solve a linear program for determining the battery storage policy for each period.

The main contribution of the proposed look-ahead framework is three-fold: (1) The proposed objective provides a real-time solution that seamlessly integrates both a non-myopic decision framework and a sequential non-parametric predictive model; (2) The FPCA-based forecast provides prediction that can capture both common daily patterns and sudden changes during a day; (3) The predictions and decisions can be updated integratively on the fly as new data is acquired. A case study is conducted with data from California ISO and the results illustrate the ease of implementation of our algorithm in practice and its capability to stabilize the power output from a wind or solar farm.

The remaining paper is organized as follows. Sec. 2 reviews relevant studies. Sec. 3 presents the stochastic control program formulation. In Sec. 4, we develop the solution procedure. In Sec. 5, we conduct a case study using data from California ISO. Sec. 8 concludes the paper.

#### 2 Literature review

Recently, considerable attention has been paid to the application of energy storage to grid system operations. In [12,13], an optimal control model is proposed for storage management under the assumption that the load (demand) and renewable energy are deterministic or perfectly known. In a dynamic and off-line setting, control strategies have been proposed to mitigate the intermittent nature of renewable energy sources [14,15]. In particular, real-time control and load prediction are integrated to solve scheduling problems. In these works, load statistics are assumed along with renewable energy arrivals. Obtaining real-time strategies for unknown renewable energy dynamics is challenging. Considering the integration of batteries and renewable energy, Lyapunov optimization techniques [16] have been employed to obtain a real-time control [17, 18]. A recent study [19] proposes a multi-scale scheduling model to coordinate a combined system of thermal generator, hydro pumped storage, battery, and intermittent renewable energy sources such as wind power and photovoltaic. Based on multi-scale ahead forecast data, the optimal power outputs are obtained by solving a mixed-integer linear programming model. However, in these studies the uncertain system dynamics are either assumed to be independent and identically distributed or known beforehand, which is unrealistic in practice.

To handle the time-varying stochastic nature of the production/demand, a scenario-based approach is often employed in the literature. This approach generates multiple scenarios, each of which represents the future trajectory of wind and solar power output. For instance, in [20] battery technology is studied from the perspective of the power system operator. The authors propose a two-step framework to analyze the value of energy storage to manage renewable resources in transmission systems. In the first stage, inspired by the approach in [21], a stochastic unit commitment model is formulated as a mixed integer linear program and solved using a predetermined set of renewable energy scenarios. In the second stage, other scenarios (out-of-sample) are generated to test the day-ahead solution obtained from the first stage, while determining a flexible operational strategy for batteries.

Similarly, in [22] and [23] optimization problems are formulated for determining the amount of energy charged into, or discharged from, the battery for each time interval. Their objective is to minimize the expected cost including energy purchase and investment or setup cost. A three-stage stochastic unit commitment model is proposed in [24] to manage power systems with renewable energy uncertainty and thermal energy storage. The first stage utilizes forecasts to determine the day-ahead operational decisions. Using multiple realizations, the second stage optimizes the expected generation costs in real time and then future operational decisions are considered in the last stage. The study in [23] investigates the California ISO data and classifies the wind and solar energy power output into 16 scenarios. In this scenario-based approach, when scenarios are chosen for a day or time block, they are typically kept fixed and cannot be changed during that time block. As a result, the scenario-based models do not have the flexibility to reflect the changes on the fly.

Another approach is to formulate the problem using stochastic control and optimization models. For example, in [25], an approximate dynamic programming algorithm is proposed to manage microgrids under uncertainties in real-time. The model is trained in a dynamic fashion using multiple scenarios, which are updated as new information arrives. An adaptive robust model is proposed in [26] to schedule energy and reserves a day-ahead, considering

bulk storage devices and wind uncertainty. The model is reformulated as a mixed-integer trilevel programming with lower-level binary variables. The resulting formulation is then solved via an exact nested column-and-constraint generation algorithm. In solving a wind energy commitment problem in the presence of storage, Kim and Powell [27] derive an analytical solution for the optimal policy under the assumption that wind follows a uniform distribution. The studies in [28] and [29] propose an approximate dynamic programming algorithm to manage a storage system integrated with a renewable energy source. A similar study in [30] aims to smooth the wind or solar power output curve via a stochastic control system. When a new wind or solar power output is observed, the control system determines the smoothed output sent to the electricity grid and the remaining excess production or shortage is covered by the battery system. However, the wind or solar farm does not provide the smoothed output before the production is observed, and thus, does not provide a commitment for the ISO/RTO where electricity generators are required to provide commitments before actual production is observed.

In summary, existing studies provide dynamic decisions or controls, assuming predictions are pre-determined *a priori*, follow a simple distribution or defined by a set of scenarios. Consequently, when actual power outputs differ from the assumed values, resulting decisions can significantly increase operational costs. On the contrary, we proposes a sequential scheme that provides and updates a predictive distribution over all time points within a horizon and exploits these functional predictions to provide forward looking decisions.

#### 3 Problem Formulation

In an electricity grid system that generates and delivers renewable energy, we consider the supply side of the system, i.e. a wind/solar farm which generates renewable energy and delivers a committed amount to a distributor. The farm uses a battery to help manage the variable renewable output of the wind/solar operator. The distributor then gathers energy from generators and then sends them to the customers. Here we present the problem with one renewable farm and one battery system (Figure 2). However, our approach is generic and can be readily extended to multiple farms or battery systems.

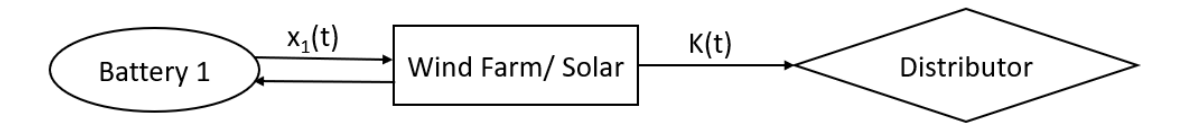


Figure 2: Wind/Solar Farm's Problem Considered in This Study

We consider that the committed dispatch levels for the wind/solar farm is determined in the day-ahead unit-commitment market. Let K(t) denote the promised amount at time t. For example, assume t to be in hours, in the day-ahead market the farm commits a certain amount of energy each hour for the next day, such that K(0), ..., K(23) are determined a day ahead. In the actual operation, the generated energy could be different than the committed amount due to the renewable source stochasticity, therefore, the farm's goal is to efficiently

manage operations, with the help of the battery, to deliver the promised amount of energy to the distributor.

Figure 2 shows the flow of energy in the wind/solar farm problem. We assume a battery is connected to the farm, named Battery 1. The amount of discharged energy of Battery 1 at time t is denoted by  $x_1(t)$ . If  $x_1(t)$  is negative, the farm charges the battery with energy  $-x_1(t)$ . Let S(t) denote the stochastic process representing the farm's energy output at time t. Then, the overall amount of energy which the farm can send to the distributor is  $S(t) + x_1(t)$ . However, it may be higher or lower than the committed amount K(t).

If  $S(t) + x_1(t) < K(t)$ , i.e. the farm cannot fulfill the promised amount, the farm must purchase the energy difference from the electricity spot market, at a unit price of  $c_{spot}(t)$  per unit (this can also be viewed as a penalty that the farm is charged). On the other hand, if  $S(t) + x_1(t) > K(t)$ , i.e. the farm produces too much energy, the farm has to salvage the excess energy at a unit price of  $c_{salvage}(t)$  per unit.

We formulate the wind/solar farm operation problem as a forward looking stochastic convex program (SCP) that minimizes the overall expected cost of the farm over a discretized rolling horizon from time period (the current period) 0 to T (the ending period). The objective is given as follows:

$$SCP : \min_{\{\boldsymbol{x}_{1}(t):t=0,\cdots,T-1\}} \sum_{t=0}^{T-1} \rho^{t} \cdot [c_{salvage}(t) \cdot E(\max\{0, S_{1}(t) - K(t)\}) + c_{spot}(t) \cdot E(\max\{0, K(t) - S_{1}(t)\})] + \rho^{T} \Phi(B(T)),$$
(1)

s.t. 
$$B(t+1) = B(t) - x_1(t),$$
 (2)

$$B_{min} \le B(t+1) \le B_{max},\tag{3}$$

$$-L \le x_1(t) \le L,\tag{4}$$

for all  $t = 0, \dots, T - 1$  with

$$S_1(t) = S(t) + x_1(t), (5)$$

where  $S_1(t)$  and K(t), respectively, represent the overall supply and demand of the farm, and  $\rho$  is the discount factor over time. Also,  $\Phi(B(T))$  is the terminal cost that depends on the final battery charge. For the terminal cost, one can simply assume it is zero for all states. Another alternative is to use  $\Phi(B(T)) = c \cdot \max\{0, b - B(T)\}$ , when there is a charge c for each unit of energy below the level b.

In the SCP above, the decision variables are  $\{x_1(t): t=0,1,\cdots,T-1\}$ ; the charged/discharged amount of energy of Battery 1. The initial energy level B(0) is known and  $B(t) \in [B_{min}, B_{max}]$  where  $B_{min}$  and  $B_{max}$  denote the capacity limits of Battery 1. Finally, the constraint in (4) limits the maximal charging/discharging rate during a time interval.

The formulation in SCP aims to optimize battery operations through quantifying and minimizing costs over a long-term rolling horizon. By solving this program, the farm owner can obtain the Battery charge/discharge decisions for each time period so that the overall expected purchase and salvage cost of the farm can be minimized.

In practice, solving (1) is extremely challenging as S(t) is unknown over the future horizon. This renders the problem extremely challenging and impractical in real-time, while in reality  $x_1(t)$  needs to be decided in an online fashion. Suppose that the current time is  $t_0$  and we need to decide Battery 1's charge/discharge amount  $x_1(t_0)$ . Now define  $S(t) \in [0, S_{max}]$  and  $B(t) \in [B_{min}, B_{max}]$  as the state space, where  $S_{max}$  is the maximal power capacity of the wind/solar farm. Also let the current renewable energy output  $S(t_0) = s$  and battery level  $B(t_0) = b$ . Using a dynamic programming approach, the value function  $V_{t_0+1}(s, b)$  under an optimal policy at time point  $t_0 + 1$  is given as

$$V_{t_0+1}(s,b) = \sum_{t=t_0+1}^{T-1} \rho^{t-t_0-1} \cdot [c_{salvage}(t) \cdot E(\max\{0, S_1(t) - K(t)\}) + c_{spot}(t) \cdot E(\max\{0, K(t) - S_1(t)\})] + \rho^{T-t_0-1} \Phi(B(T)).$$
(6)

With the optimal value function  $V_{t_0+1}^*(s,b)$ , the SCP at time  $t_0$  is solved as a stochastic dynamic model,  $SDP(t_0)$ :

$$SDP(t_0): V_{t_0}(s, b) = \min_{x_1(t_0)} c_{salvage}(t_0) \cdot \max\{0, s + x_1(t_0) - K(t_0)\}$$

$$+ c_{spot}(t_0) \cdot \max\{0, K(t_0) - s - x_1(t_0)\}$$

$$+ \rho \int_{c^* - 0}^{S_{max}} V_{t_0 + 1}^*(s^*, b - x_1(t_0)) p_{ss^*}^{(t_0)} ds^*$$

$$(7)$$

s.t. 
$$B_{min} \le b - x_1(t_0) \le B_{max},$$
 (8)  
-  $L < x_1(t_0) < L.$  (9)

where  $p_{ss^*}^{(t_0)} := P(S(t_0 + 1) = s^* \mid S(t_0) = s)$  is the transition probability at time  $t_0$  from wind/solar power output s to  $s^*$ . In practice these probabilities are unknown and need to be estimated for each state s at every time t. One possible approach to obtain each  $p_{ss^*}^{(t)}$ ,  $t = 1, 2, \dots, T - 1$  is to assume S(t) follows a stochastic differential equation governed by a Brownian motion, and then solve a set partial differential equation (using the Kolmogorov forward equation [31]). Besides the independent increment assumption inherited from the Brownian motion, this approach is not unsuitable for an online application.

Furthermore, solving  $SDP(t_0)$  requires a computationally expensive and time consuming backward dynamic procedure which computes the optimal immediate policy  $x_1(t)$ , as a function of the state variables S(t) and B(t) at each epoch  $t = T, T - 1, \dots, t_0$ . Moreover, during the implementation, as is usual in stochastic dynamic programming, at each epoch  $t = t_0, 1, \dots, T - 1$ , the optimal action as a function of the states, is selected from a look-up table and implemented. This procedure is thus not adapted to the changing circumstances encountered during the implementation and is only valid in case the dynamic process is stationary and homogeneous.

# 4 The Deterministic Solution and Stochastic alternatives

We first present the linear programming formulation in Section 4.1 where we relax the problem using the Jensen's inequality and decide the battery charging/discharging operations given the future S(t). Because the future S(t) is unknown, in Section 4.2 we provide a prediction method based on FPCA and highlight its advantages over other predictive techniques. Once the prediction is made, we solve the linear problem in Section 4.1 with the predicted S(t). In doing so, to minimize the influence of the prediction uncertainty, we only execute the decision for time t and proceed to the next epoch and update the prediction with the most recent data. This process is repeated until we reach the last epoch. In Section 4.3 we summarize the overall framework.

#### 4.1 Linear Programming

In this section we present a solution procedure for approximately solving the SCP. Note that  $\max\{0, S_1(t) - K(t)\}$  and  $\max\{0, K(t) - S_1(t)\}$  in the SCP objective function are convex. Therefore, we can employ the Jenson's inequality to obtain the lower bound of the objective function. Specifically, we obtain

$$c_{salvage}(t) \cdot E\left(\max\{0, S_{1}(t) - K(t)\}\right) + c_{spot}(t) \cdot E\left(\max\{0, K(t) - S_{1}(t)\}\right)$$

$$\geq c_{salvage}(t) \max\{0, E(S_{1}(t)) - K(t)\} + c_{spot}(t) \cdot \max\{0, K(t) - E(S_{1}(t))\}.$$
(10)

This inequality implies that we can relax the problem by replacing the original objective function in (1) with its lower bound and solve the problem that can minimize the bound. Such relaxation provides us a new objective function as

$$\sum_{t=0}^{T-1} \rho^{t} \cdot [c_{salvage}(t) \max\{0, E(S_{1}(t)) - K(t)\} + c_{spot}(t) \cdot \max\{0, K(t) - E(S_{1}(t))] + \rho^{T} \Phi(B(T)),$$
(11)

This reformulation renders the optimization problem as a deterministic piecewise-linear optimization, given the 'max' operators. Let us further define the auxiliary variables  $O_{excess}(t)$  and  $O_{shortage}(t)$  that represent the energy excess and shortage, respectively, at the decision epoch t. Then we can reformulate the problem as the equivalent linear formulation (LP) with linear inequality constraints of the piecewise objective. This results in the linear minimization program over the auxiliary variables and the decision variables. Suppose that the current time is  $t_0$ . Then the LP formulation is given as follows.

$$LP(t_0) : \min \sum_{t=t_0}^{T-1} \rho^{t-t_0} \cdot [c_{salvage}(t) \cdot O_{excess}(t) + c_{spot}(t) \cdot O_{shortage}(t)] + \rho^{T-t_0} \Phi(B(T))$$

$$(12)$$

$$s.t. \quad O_{excess}(t) \ge E(S(t)) + x_1(t) - K(t), \tag{13}$$

$$O_{shortage}(t) \ge K(t) - E(S(t)) - x_1(t), \tag{14}$$

$$O_{excess}(t), O_{shortage}(t) \ge 0,$$
 (15)

$$B(t+1) = B(t) - x_1(t), (16)$$

$$B_{min} \le B(t+1) \le B_{max},\tag{17}$$

$$-L \le x(t) \le L. \tag{18}$$

for all  $t = t_0, t_0 + 1, \dots, T - 1$ . Here, note that the shortage and excess functions in the objective function in (6), which are piecewise linear and convex, have been linearized in this formulation.

From  $LP(t_0)$ , we observe that we only need to estimate  $\{E(S(t)): t = t_0 + 1, ..., T - 1\}$  to calculate the decision variables at each epoch. This greatly simplifies the estimation procedure, compared to the original formulation SCP where  $E(\max\{0, S_1(t) - K(t)\})$  and  $E(\max\{0, K(t) - S_1(t)\})$  need to be estimated. In the following section we present a non-parametric Bayesian approach, based on FPCA, that can estimate (and update) E(S(t)) and seamlessly integrate the FPCA forecasts with (12). The key advantage of the FPCA is that E(S(t)) over the future horizon can be updated on the spot as more data is observed. Thus, at each time epoch, predictions are updated and hence the decisions. This allows us to refine decisions over time as more data is gathered and account for non-stationary behavior with sudden changes in the renewable supply.

Finally we note that in (12), the LP is written as  $LP(t_0)$ . The reason is that, despite the fact that solving  $LP(t_0)$  results in the optimal  $\boldsymbol{x}^*(t) = \{x_1^*(t_0), \cdots, x_1^*(T-1)\}$ , these decisions are updated at the next epoch as new data is observed. Thus at decision epoch t only  $x_1^*(t)$  is implemented. More detailed discussion will be provided in Sec. 4.3.

## 4.2 Real-time Functional Principal Component Analysis

Because the future movements of S(t) are unknown to the farm, and we make no assumption on the nature of their stochastic dynamics, we propose to predict the future values of S(t) with FPCA and use the predicted values in  $LP(t_0)$ . We note that any predictive approach can be plugged (ex: Neural networks, Arima, etc...) into our method yet the main advantages of our FPCA approach are:

- Non-Parametricity: The intermittency and high volatility of renewable energy makes predictions highly vulnerable to model mis-specifications. Further, no physical equations are currently available that provide an accurate prediction for renewable energy. Hence, we believe a non-parametric approach is suitable for such applications.
- Model Updating: A salient aspect of FPCA is that, despite non-parametricity, it features a linear and orthogonal decomposition of longitudinal signals which in turn facilitates efficient model updating using an empirical Bayes procedure. Indeed, this decomposition makes it viable in situations that require fast decisions (such as the operational decision-making per every 5 minutes in our case study).
- Heterogeneity: FPCA has proven itself to be specifically competitive when functions pose some heterogeneity. The volatility of renewable energy requires this capability.

• Functional inference: FPCA is an operator on the functional space. It borrows the strength across a set of functions to improve prediction performance for the function at hand. As a result, it can provide competitive predictive capabilities for both short and long term predictions within its predefined domain.

To achieve real-time predictions, the energy supply data is divided by day to form a longitudinal dataset. Then, the supply for the period running from current time to the end of current day is predicted. And, as more supply data is collected, the prediction for the day is then updated using an empirical Bayesian approach. Specifically, without loss of generality, consider  $t \in [0, 24)$ , i.e. horizon spans a day which is the case in the day-ahead unit-commitment market. Suppose that the current time is  $t_0$  where the value of S(t),  $t \leq t_0$  for some  $t_0 \geq 0$  is observed. Further, suppose we start with the first prediction cycle as day 0. Let us define  $S^{(-j)}(t)$  as the farm output at time t, j days before day 0. Therefore,  $\{S^{(-j)}(t) \mid j=1,\cdots,J,t=1\cdots,T\}$  forms the training data with data collected during the past J days. Now in day 0, given the observation  $S(1),\cdots,S(t_0)$ , our goal is to estimate the future values of E(S(t)) over the rolling horizon, i.e.,  $E(S(t_0+1)),\cdots,E(S(T-1))$ . Here note that  $S(t) \triangleq S^{(0)}(t)$  which denotes the supply output in the current day.

Now assume that  $\{S^{(-j)}(t)\}_{j=1}^J$  for  $t \in \mathcal{T}$  are generated from a square-integrable stochastic process  $\bar{S}(t)$  such that  $\mathcal{T}$  stands for a time domain. FPCA decomposes  $\bar{S}(t)$  as

$$\bar{S}(t) = \mu(t) + \sum_{k=1}^{\infty} \xi_k \phi_k(t) + \epsilon(t), \tag{19}$$

where  $\mu(t) = E(\bar{S}(t))$ ,  $\epsilon(t) \sim \mathcal{N}(0, \sigma^2)$  and  $\xi_k = \int_{\mathcal{T}} (\bar{S}(t) - \mu(t)) \phi_k(t) dt$  is the functional principal component (FPC) score associated with eigen function  $\phi_k(t)$ . The FPCA scores are pairwise-independent random variables with zero mean and variance  $\lambda_k$  (i.e.  $E(\xi_k^2) = \lambda_k$ ). Here  $\lambda_k$  denotes the Eigen values associated with the Eigen functions and are ordered by  $\lambda_1 \geq \lambda_2 \geq \cdots \geq 0$ . As is shown in (19), heterogeneity across the population is encoded via the different eigenfunctions and their corresponding coefficients, i.e., the eigen scores  $\xi_k$ . To achieve a finite representation, only the largest K eigen values are considered such that  $S^{(-j)}(t) \approx \mu(t) + \sum_{k=1}^K \xi_{jk} \phi_k(t) + \epsilon(t)$  for  $j \in \{1, ..., J\}$ . We follow standard procedures in [32] to estimate model parameters; the mean function  $\mu(t)$ , eigen functions  $\phi_k(t)$ , and variances  $\lambda_k$ .

Given the model above, our goal is to predict S(t) given new observations  $\{S(1),...,S(t_0)\}$ . In particular, we aim to reflect the general trend from previous days, but at the same time, individualize the predictions to data from the specific day under consideration. Specifically, the curve for the estimated output for the current day (day 0) is represented as  $S(t) = \mu(t) + \sum_{k=1}^{K} \xi_{0k} \phi_k(t) + \epsilon(t)$ , where  $\xi_{0k}$  are the FPC scores of S(t). Now the prediction of S(t) can be achieved by estimating  $\xi_{0k}$ . To this end, we exploit empirical Bayesian updating scheme. Specifically, we utilize the trained  $\lambda_k$  as prior on  $\xi_{0k} \sim \mathcal{N}(\xi_{0k}; 0, \lambda_k)$  for k = 1, ..., K. This prior reflects the general trend we infer from previous days. We then derive the posterior

$$P(\xi_{01},...,\xi_{0K}|S(1),\cdots,S(t_0)) = \mathcal{N}(\xi_{01},...,\xi_{0K};\boldsymbol{\xi}^*,\boldsymbol{\Sigma}^*),$$
(20)

where

$$egin{aligned} oldsymbol{\Sigma}^* &= \left(rac{1}{\sigma^2}\Phi(oldsymbol{t})'\Phi(oldsymbol{t}) + oldsymbol{\Lambda}^{-1}
ight)', \ oldsymbol{\xi}^* &= rac{1}{\sigma^2}oldsymbol{\Sigma}^*\Phi(oldsymbol{t})'ig(\mathbf{S}(oldsymbol{t}) - oldsymbol{\mu}(oldsymbol{t})ig) \end{aligned}$$

with

$$\mathbf{S}(\boldsymbol{t}) = (S(1), ..., S(t_0))', \qquad \boldsymbol{\mu}(\boldsymbol{t}) = (\mu(1), ..., \mu(t_0))',$$

$$\boldsymbol{\Lambda} = \operatorname{diag}(\lambda_1, ...\lambda_K), \qquad \boldsymbol{\Phi}(\boldsymbol{t}) = \begin{bmatrix} \phi_1(1) & ... & \phi_K(1) \\ \vdots & \ddots & \vdots \\ \phi_1(t_0) & ... & \phi_K(t_0) \end{bmatrix}.$$

Given the posterior distribution (20), the predictive mean  $E_{t_0}(S(t)|S(1), \cdots S(t_0)) \triangleq S_{t_0}^*(t)$  and variance  $var_{t_0}(S(t)|S(1), \cdots S(t_0)) \triangleq \sigma_{t_0}^{2*}(t)$  for time  $t = t_0 + 1, ..., T - 1 \in \mathcal{T}$  are given as:

$$S_{t_0}^*(t) = \mu(t) + \sum_{k=1}^K [\boldsymbol{\xi}^*]_k \phi_k(t),$$

$$(\sigma_{t_0}^*(t))^2 = \hat{\sigma}_{\mu}^2(t) + \sum_{k_1}^K \sum_{k_2}^K [\boldsymbol{\Sigma}^*]_{k_1, k_2} \phi_{k_1}(t) \phi_{k_2}(t) + \hat{\sigma}^2(t),$$
(21)

where  $\hat{\sigma}_{\mu}^{2}(t)$  is estimated variance of  $\mu(t)$ . The result above is key to our model as it implies that updating predictions can be efficiently done in closed form, following the linearity (in reference to coefficients) of the FPCA decomposition. Real-time updating in turn allows us to refine our decisions, also in real-time, due to the efficiency of the LP construction. This fact and the overall algorithm steps are highlighted in the following subsection. Here we note that in the appendix we add some practical considerations for fitting FPCA.

#### 4.3 Overall Decision Framework

As shown in Algorithm 1, at each time epoch the farm can solve the linear program LP(t) to decide the amount of energy that should be charged into (or withdrawn from) the battery set,  $x_1^*(t)$ . Note that solving LP(t) results in optimal decisions over the entire horizon  $\boldsymbol{x}^*(t) = \{x_1^*(t_0), \cdots, x_1^*(T-1)\}$ . If we exactly knew the future S(t) over the future horizon then  $\boldsymbol{x}^*(t)$  would be optimal. However S(t) is predicted and at the next epoch the predictions are updated and hence the decisions. As such, at time t only the first optimal solution  $x_1^*(t)$  is implemented. The dynamic approximation algorithm for solving  $LP(t_0)$  is given in Algorithm 1.

#### 4.4 Stochastic Alternatives

One key advantage of FPCA is that it provides a full predictive distribution. This implies that stochasticity in S(t) over the entire horizon can be accommodated for in our model. Here

#### Algorithm 1 The Dynamic Approximation Algorithm For The Wind/Solar Farm Problem

- 1: FPCA Training Steps:
- 2: Train the FPCA in (19) using previous J days' data  $\{S^{(-j)}(t) \mid j=1,\cdots,J,t=1\cdots,T-1\}$ .
- 3: Decision Making Steps:
- 4: **for** t = 1 to T 1 **do**
- 5: Observe the renewable power output at current time t: S(t).
- 6: Update the FPCA model using the observed data  $S(1), \dots, S(t)$  and (20).
- 7: Predict  $S_t^*(t+1), \dots, S_t^*(T-1)$  using (21).
- 8: Solve the linear program LP(t) in (12) with the predicted power output.
- 9: Use the first optimal solution  $x_1^*(t)$  as the battery charge/discharge decision at time t.
- 10: end for

we propose two alternative solutions (i) a scenario based approach (ii) a robust optimization approach. We will defer the robust approach to the appendix and focus on the scenario based approach.

Recall, that our Empirical Bayes approach yields a posterior  $P(\xi_{01},...,\xi_{0K}|S(1),\cdots,S(t_0)) = \mathcal{N}(\xi_{01},...,\xi_{0K};\boldsymbol{\xi}^*,\boldsymbol{\Sigma}^*)$  after each data point is collected. Hence at any time point, a possible scenario for the evolution of S(t) over the future horizon can be generated through sampling from  $\mathcal{N}(\xi_{01},...,\xi_{0K};\boldsymbol{\xi}^*,\boldsymbol{\Sigma}^*)$  and finding the predictive mean in (21) over the future horizon;  $t \in \{t_0 + 1,...,T-1\}$ . Therefore, a stochastic alternative of our expectation approach in (12) is shown in (22).

$$\min \frac{1}{N} \sum_{i=1}^{N} \left\{ \sum_{t=0}^{T-1} \rho^{t} \cdot \left[ c_{salvage}(t) \cdot (O_{excess}^{(i)}(t) + O_{B}^{(i)}(t)) + c_{spot}(t) \cdot (O_{shortage}^{(i)}(t) + U_{B}^{(i)}(t)) \right] + \rho^{T} \Phi(B_{i}(T)) \right\},$$
(22)

$$s.t. \quad \hat{x}_{i}(t) = x(t) + O_{B}^{(i)}(t) - U_{B}^{(i)}(t),$$

$$B_{i}(t+1) = B_{i}(t) - \hat{x}_{i}(t),$$

$$-L \leq \hat{x}_{i}(t) \leq L,$$

$$O_{excess}^{(i)}(t) \geq S_{i}(t) + \hat{x}_{i}(t) - K(t),$$

$$O_{shortage}^{(i)}(t) \geq -S_{i}(t) - \hat{x}_{i}(t) + K(t),$$

$$O_{excess}^{(i)}(t), O_{shortage}^{(i)}(t) \geq 0,$$

$$O_{B}^{(i)}(t) \geq B_{i}(t) - x(t) - B_{max},$$

$$U_{B}^{(i)}(t) \geq B_{min} - (B_{i}(t) - x(t)),$$

$$O_{B}^{(i)}(t), U_{B}^{(i)}(t) \geq 0,$$

$$B_{min} \leq B_{i}(t+1) \leq B_{max},$$

for all  $t = 0, \dots, T - 1$ 

A key feature of this approach is the automatic selection of relevant scenarios. By automatic, we imply that FPCA can inherently update the posterior as new data comes in and hence the posterior will reflect possible scenarios relevant to data collected at the specific time of interest. We note that in (22), there is a general battery charging/discharging decision variables x(t) and the scenario-based ones  $\hat{x}_i(t)$ . x(t) is the guiding decision for all scenarios, but it may not be feasible for a specific scenario because of the stochasticity of the energy output. Therefore, we construct the scenario-based decision  $\hat{x}_i(t)$  using decisions X(t) that are feasible for each scenario.

Similarly, we can also build a robust optimization approaches, whose objective function is the largest cost among all N scenarios. The formulation and results are presented in Appendix.

## 5 Case Study Preliminaries

In this section, we apply the proposed method on data from the California ISO [33]. The dataset includes the amount of energy generated from several types of sources (i.e., wind, solar, thermal, nuclear, and hydro) and the load. It covers a span of several years (2014-2019), collected daily at 5-minute intervals. Table 1 shows a sample of the dataset available in [33].

Date	Hour	Interval	Load	Solar	Wind	Net Load	•••
1/1/2019 0:00	1	1	22,320	0	2,862	19,458	
$1/1/2019 \ 0.05$	1	2	22,295	0	2,915	19,380	
1/1/2019 0:10	1	3	22,204	0	2,919	19,285	• • •
÷	:	:	:	:	:	:	:
1/1/2019 6:50	7	11	21,644	3	2,034	19,607	
1/1/2019 6:55	7	12	21,613	52	2,026	19,535	
1/1/2019 7:00	8	1	21,655	121	2,020	19,514	• • •
:	•	:	:	•	•	:	:

Table 1: California ISO Data Set (in Megawatts)

In Table 1, the "Load" column represents the actual electricity consumption during a 5-minute interval. The "Solar" and "Wind" columns show the energy production from solar and wind farms, respectively. The "Net Load" is the actual load minus solar and wind production. The net load is met by other energy sources, typically expensive conventional power plants. Other columns include energy production from other sources, for example, thermal, hydro, nuclear, imports, etc.

#### 5.1 Data Exploration

We first provide illustrative examples that highlight some components of the California ISO data. Figure 3 presents the solar plus wind power production data for each day of a month, each represented by a different colored curve. We observe that the daily solar and wind power production have strong commonalities and follow a similar pattern. This observation suggests that a prediction model that captures the common diurnal pattern could be beneficial for non-myopic decision making. On the other hand, the pattern varies day-by-day, so the prediction model should take into consideration such variations for accurate short-term predictions. This can be achieved via our FPCA model which starts off by a population estimate in (19) and then individualizes the daily predictions in real-time in (20).

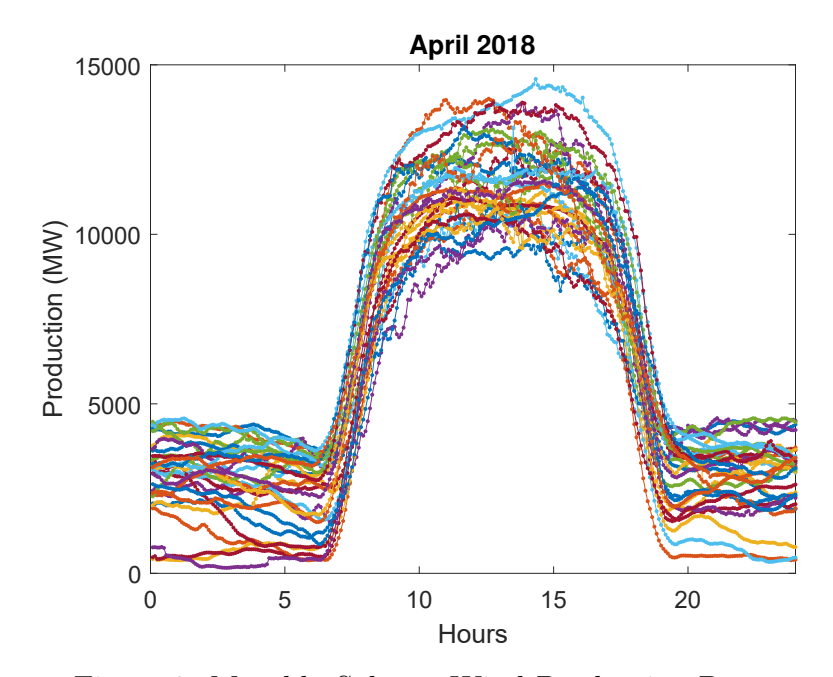


Figure 3: Monthly Solar + Wind Production Data

Figure 4 presents the wind (in red lines) and solar (in blue lines) power production during a specific day on April 2018. The green area represents the amount of energy curtailed by the ISO. The solar plants generate the largest amount of energy at around noon, while producing zero energy at night. On the other hand, the wind system generate more power at night. We also observe that seasonally, solar power production is high in the summer and low in the winter. Overall, the power production from the solar plants is larger than the power generated by the wind farms in this case study. Curtailment often occurs when the power production is unexpectedly large. For example, in April 17, 2018, about 15% of solar power production was curtailed.

Here we note that the Duck curve in Figure (1), can be directly recovered from subtracting wind and solar power generation from the total load, i.e., the net load. Also, we recall that in order to supply the large rump-up of energy caused by the Duck curve (at around 3pm) the California ISO runs conventional plants at low generation capacity at noon.

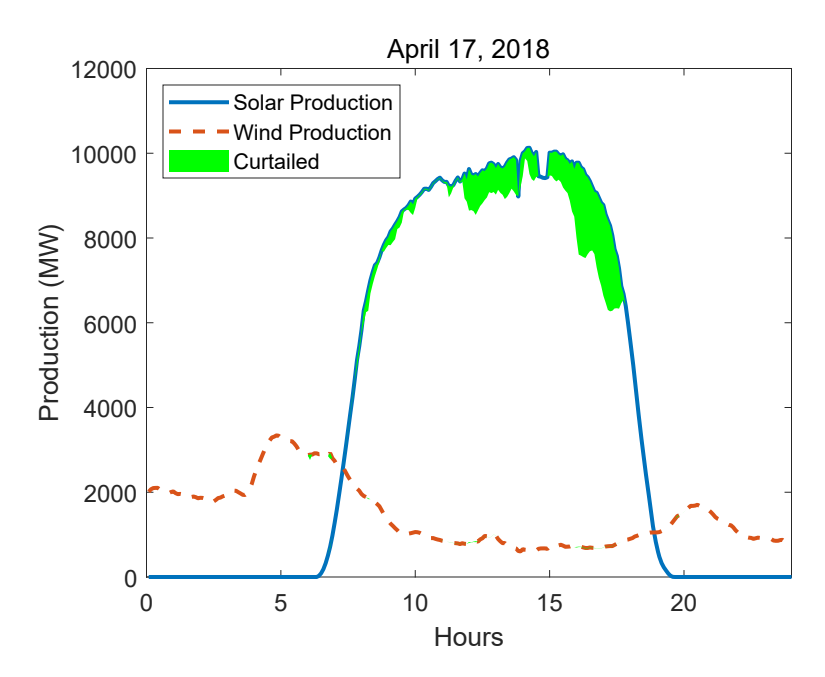


Figure 4: A Daily Sample of Solar and Wind Production Data

#### 5.2 Illustration of FPCA Prediction

Figure 5 presents the FPCA prediction results for wind and solar power production for April 27. The horizontal axis denotes time of day in minute scale and the vertical axis denotes power output from the farm. The prediction is made, based on observed data within the day. For example, in the left figure, data up to 4:10 AM (250 minute) is known and the FPCA model uses this information to predict the days trend.

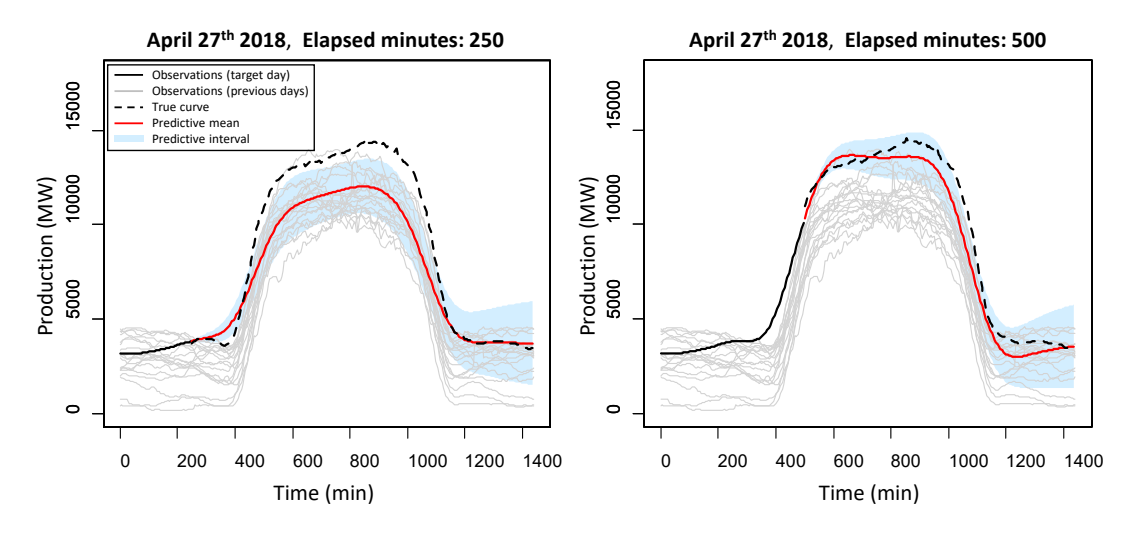


Figure 5: FPCA Prediction Results for Wind+Solar Production

We observe that FPCA can yield competitive predictions over the entire horizon. At the 4:10 AM, the trend still follows the overall population mean. This is intuitively understandable as few data is collected at that day. However, as more data is gathered, predictions

are individualised and reflect better the day at hand. This can be seen from predictions after 500 minutes elapsed throughout the day. Also notice that as more data is gathered the predictive distribution becomes more accurate and more concentrated; hence the previously mentioned notion of automatic selection of the relevant scenarios.

#### 5.3 Benchmark Methods and Evaluation Metrics

For our non-myopic approach with FPCA predictions, we compare three alternatives of our model. Those are:

- Expectation approach given in (12).
- Scenario approach given in (22).
- Robust approach given in (26).

We also benchmark with

- Non-myopic approach with perfect forecast: We assume that S(t) is fully know  $\forall t \in \{0, \dots, T-1\}$  and denote the deterministic function as  $S^{\text{true}}(t)$ . We then optimize the objective in (12) at  $t_0 = 0$  to obtain  $\boldsymbol{x}^*(0) = \{x_1^*(0), \dots, x_1^*(T-1)\}$ . Note that no updating is performed in this approach, since S(t) is known and thus the initial set of decisions  $\boldsymbol{x}^*(0)$  are optimal.
- Myopic approach with perfect forecast: The charging/discharging decision at time  $t_0$  is made with only the knowledge of the farm output observation  $S(t_0)$ , but no future information is taken into consideration. In other words, the problem is solved by taking a snapshot of the system. To do this the sum notation in (12) is removed and the " $t = t_0, \dots T 1$ " in the constraints are replaced by " $t = t_0$ ". This one-period linear programming is easy to solve. Its decision can be stated as:
  - When the farm output  $S(t_0)$  is greater than the promised output  $K(t_0)$  and the battery is not yet full, the battery is charged until the overall output  $S(t_0) + x_1(t_0)$  equals the promised output  $K(t_0)$  or the battery becomes full.
  - When the farm output  $S(t_0)$  is less than the promised output  $K(t_0)$ , and if the battery is not yet empty, the battery is discharged until the overall output  $S(t_0) + x_1(t_0)$  equals the promised output or the battery becomes empty.
  - No charging/discharging action is made if the two rules above are not satisfied.
- Myopic approach with FPCA forecast: This is similar to the prefect forecast one, but without knowing the true observation of the farm output at  $t_0$ . Instead FPCA is used to predict  $S(t_0)$ . Note that here any of the expectation, robust or scenario approaches can be used to obtain decisions.

A regret ratio metric is defined to compare model performance. We first define regret  $f \in \mathbb{R}^+$  as the total cost incurred from excess production and shortage from time 0 to T-1

$$f = \sum_{t=0}^{T-1} [c_{salvage}(t) \cdot \max\{0, S^{true}(t) + x_1^*(t) - K(t)\}$$

$$+ c_{spot}(t) \cdot \max\{0, K(t) - S^{true}(t) - x_1^*(t)\}].$$
 (23)

Given, (23), it is clear that the non-myopic method under perfect forecast considers the most accurate and largest amount of information, as it optimizes over a long-term horizon with perfect knowledge of the supply evolution. Based on this, regret ratio is defined as

regret ratio = 
$$\frac{f - f_0}{f_0}$$
, (24)

where  $f_0$  denotes the cost of the reference method. Note that for simplicity of interpretation, but without loss of generality, we use the zero terminal cost.

#### 5.4 Settings

The following parameters are set.

K(t)	7,500 MW
$B_{min}^{(1)}$	1,500 MWh
$B_{max}^{(1)}$	15,000 MWh
$B_1(1)$	7,500 MWh
$L_1$	9,000 MWh
$c_{salvage}$	0.50
$\rho$	1

The spot price,  $c_{spot}(t)$ , varies over time. Usually the electricity price is high in the early morning and evening because the demand is high and production is lower. We use the average 5-minute ahead marginal prices in the California electricity market available in [34]. Figure 6 presents the used market price.

## 6 Proof of Concept: Effect of Look-ahead Planning

This section presents a proof of concept that illustrates the advantage of look-ahead planning. To this end, we only consider the non-myopic and myopic methods under perfect forecast. We understand that the perfect forecast assumption is not realistic, but it eliminates prediction errors so we can gain useful insights on how the proposed forward-looking approach affects the decision-making process. Note here that since predictions are deterministic, only the expectation approach can be used. In addition, the discounting factor is set to  $\rho = 1$ . As a result, the difference between both methods is purely caused by the far-horizon information.

We consider two different scenarios on the spot price. Figure 7 depicts the results for the non-myopic and myopic methods under the perfect forecast assumption with varying spot prices obtained in [34], whereas Figure 8 considers a constant spot price at  $c_{spot} = 3$ . The horizontal axis is time and the vertical axis is energy output. The dashed horizontal line implies the committed energy by the farm (e.g., decided from the day-ahead unit-commitment). The blue curve is the power generated from the wind/solar power plant and the red curve represents the amount of energy withdrawn from the battery. The black curve is the farm output  $S_1(t)$  which is equal to the wind/solar (S(t)) plus the battery charge/discharge amount

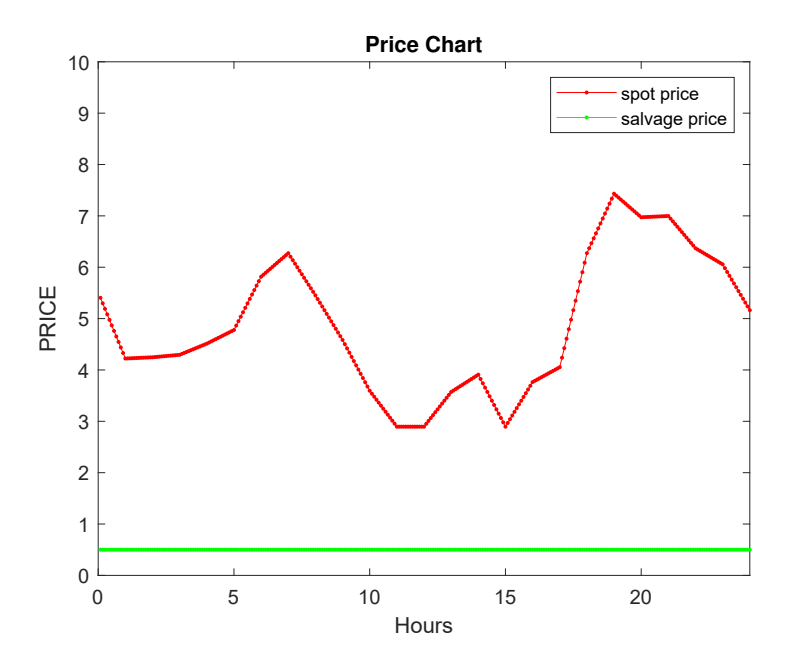


Figure 6:  $c_{spot}$  and  $c_{salvage}$  over the day

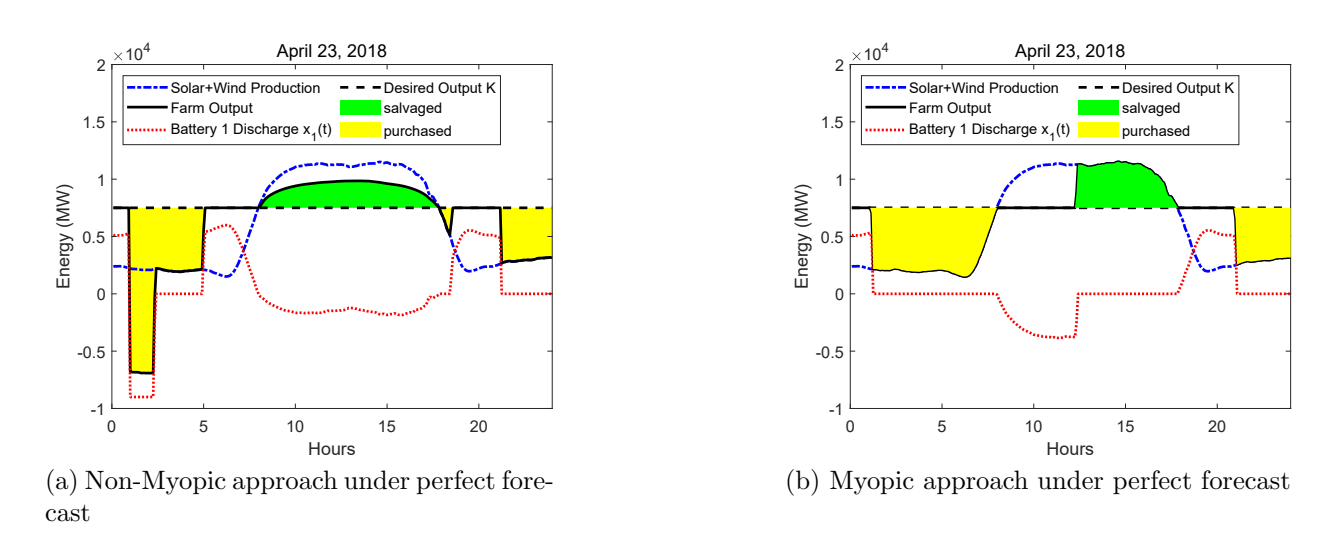
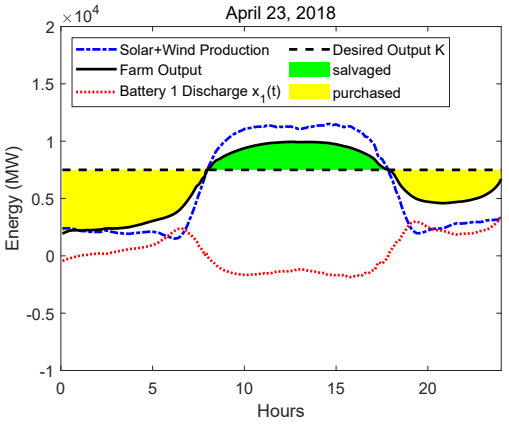


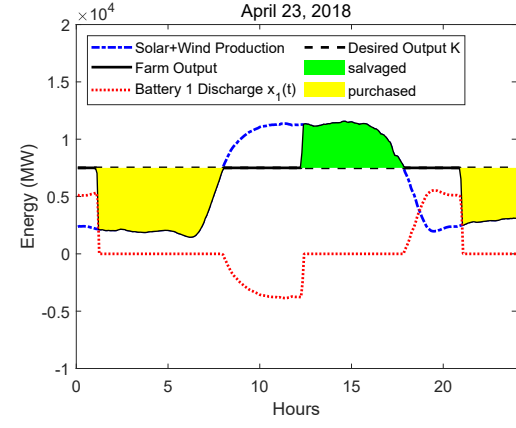
Figure 7: Results with varying spot prices and no discounting factor, i.e.  $\rho = 1$ , under perfect forecast

 $x_1(t)$ . Table 2 provides the regret ratio of the myopic approach, compared to the non-myopic approach in Figures 7 and 8.

Table 2: Regret ratios for the myopic method under two different spot price scenarios in Figures 7 and 8

Varying spot price	constant spot price		
8.42 %	0%		





(a) Non-Myopic approach under perfect forecast

(b) Myopic approach under perfect forecast

Figure 8: Results with constant spot prices and no discounting factor, i.e.  $\rho = 1$ , under perfect forecast

The curves in the figures explains how the objective function, i.e. the overall cost from excess production and shortage, is calculated. When the black solid curve is above the black dashed line, the overall output from the farm is higher than the committed amount, so the farm should salvage the excess production, incurring the salvage cost. The salvaged energy is marked in green area in each figure. On the other hand, when the black solid line is below the black dashed line, the overall output from the farm is lower than the promised amount, so the farm purchases energy from the electricity spot-market to fill the gap, which is marked as yellow in each figure. To be more specific, let us split the 24 hours into three periods: (i) before 9:00, (ii) 9:00 to 17:30, and (iii) after 17:30. In the first and the third periods, the wind and solar output is lower than the promised amount of energy. In the second period, the wind and solar output is higher. Therefore, We observe that battery discharging (when red lines are above zero) occurs in periods (i) and (iii), while battery charging (when red lines are below zero) occurs in period (ii), except to the time between 1:00 to 2:00 in Figure 7(a).

Interestingly, Figure 7(b) and Figure 8(b) are identical. It means that the spot price does not affect the myopic method. In both subfigures, the decisions are to immediately charge (or discharge) the battery to meet the promised output until the battery is full (or empty). After the battery reaches zero (or full) capacity, the farm starts purchasing or salvaging energy. The overall cost from Figure 7(b) is higher than that in Figure 8(b), simply because the varying spot price in Figure 6 is always higher than the constant spot price  $c_{spot} = 3$ .

Another interesting aspect is that Figures 8(a) and 8(b) have the same overall cost, causing 0% regret ratio, even though the shape of the curves is different. This result confirms that if the spot cost is constant throughout the day, then myopic and non-myopic algorithms will lead to the same cost. Despite the different shapes, the decisions in Figure 8(a) and 8(b) share some common features: during periods (i) and (iii) the battery is discharged until it becomes empty, and it is charged to full capacity in period (ii), because in this way the size of yellow and green areas, which incur cost to the farm, can be minimized. Since the spot and salvage prices are constant over time, the overall costs generated by energy purchase (shown

as yellow areas) and energy salvage (shown as green areas) are the same in the two methods. However, the difference is that, because the non-myopic method in Figure 8(a) considers information in the far horizon, it averages the remaining energy (or the remaining capacity) in the battery to the whole period. Therefore, the curves in Figure 8(a) are smoother when compared to those in Figure 8(b).

Lastly, Figures 7(a) and 8(a) share identical results in period (ii), because the salvage costs are the same (and constant) in both subfigures. However, the decisions in period (i) and (iii) are different. In Figure 7(a), because the spot price is varying, the non-myopic method purchases less (or more) energy when the spot price is high (or low). As we can observe, battery is discharged and no energy is purchased during 0:00 to 1:00, 5:00 to 9:00, and 19:00 to 22:00, when the spot price is relatively high. When the spot price is low, energy is purchased through the spot market to fulfill the committed energy output. During 1:00 to 2:00, because the spot price is low, the farm decides to purchase energy and charge them into the battery. On the other hand, in Figure 8(a), because the spot price is constant, the farm has the same cost whenever it purchases energy.

From the above discussions, we can understand the differences between both approaches and the benefits of the non-myopic approach. In summary, during periods (i) and (iii) the decision in Figure 7(a) incurs much less cost because the non-myopic method considers the future information and price changes. In period (ii), the curves in Figure 7(a) are smoother because of the non-myopic property and the constant salvage price. On the other hand, when the spot and salvage prices are all constant, both the non-myopic and myopic approaches incur the same cost even though the decision over time differ, as shown in Figures 8(a) and 8(b). These results suggest that the non-myopic property can help decrease the farm's cost if the unit cost of purchasing or salvaging energy is changing in the future.

## 7 Case Study Results

The proof of concept was done under perfect predictions. Here we observe the results in a real-life setting where FPCA forecasts are used to obtain predictions. Tables 3, 4, 5 and 6 compare the regret ratios for non-myopic and myopic methods (expectation, robust and scenario based methods) under varying spot prices and  $\rho = 0.999$ . The results are shown in terms of regret ratios over multiple days in April 2018. As the load pattern during week-days are different from that on weekends, we focus our implementation on weekdays, so the analysis for weekends (e.g., April 21, 22, 28 and 29) are omitted. In addition, Table 7 summarizes the running time of each approach using a standard desktop computer. An illustration of the expectation method performance with varying spot prices with a discounting factor  $\rho = 0.999$  is given in Figure 9.

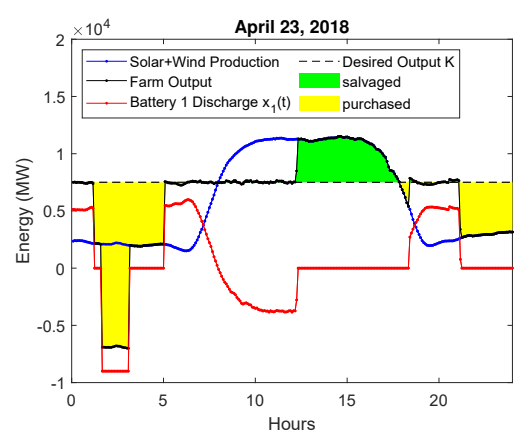
Many interesting insights can be derived from the Tables:

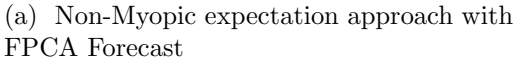
- First and most importantly, no matter which optimization formulation is used, a non-myopic framework can significantly decrease regret and hence operational costs. This in turn confirms the advantageous properties of our dynamic and non-myopic framework that can be applied under different inference procedures.
- Second, interestingly, we observe that the scenario-based approach is able to slightly

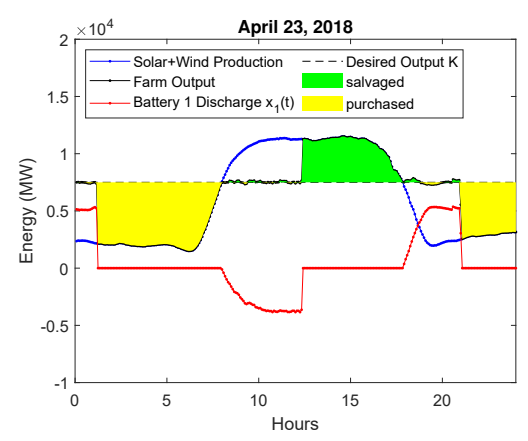
outperform the expectation-based approach when the number of scenarios is large. This is intuitively understandable because it can account for prediction uncertainty with multiple scenarios (rather than using one expected trajectory in the expectation-based approach) within our decision framework. The caveat, however, is that accounting for such uncertainty comes at the expense of increase computational times. For instance, the running time to make storage decisions increases from around 2.4 minutes to 28 minutes (refer to Table 7) when switching from expectation-based formulation to the scenario-based formulation with 10 scenarios. For the 5-min time interval considered in this study, Scenario-10 is hence an unfeasible option. We can also imagine that the scenarios-based approach is not scalable to solve large-scale problems with multiple renewables and batteries.

- Third, the Robust approach leads to worst case regret. This is expected, as we are taking decisions under worst case supply scenarios. The Robust approach provides very conservative decisions, increasing operational costs.
- Finally, from these results, while the proposed framework is flexible enough to include different optimization formulations, the expectation approach appears to be most adequate in terms of operational cost and running time.

Figure 9 also echoes our results. Through comparing subfigures 9(a) and 9(b), we observe the benefit of far-horizon planning where in period (i), the farm purchases more energy when the spot price is low and uses it when the spot price is high. This results in a smaller regret (or cost), compared to the myopic approach (see Tables 3 and 4). Also, in comparison with the non-myopic approach under perfect forecast (Figure 7(a)), we find that the major difference happens in period (ii), where the salvaging happens only in the later part of the period in Figure 9(a). This difference is due to the use of a discount factor in this setting. Since, the unit cost of salvaged energy is  $\rho^{t-t_0}c_{salvage}$ , which is decreasing over time t. Thus, in period (ii), the farm prefers to salvage its excess energy later, when the unit cost is lower.







(b) Myopic expectation approach with FPCA Forecast

Figure 9: Results with varying spot prices and a discounting factor  $\rho = 0.999$ 

#### 8 Conclusion

This paper presents a practical and easy to implement methodology for managing the output of a wind/solar farm in a cost effective and real-time manner. Our problem aims at deciding the amount of energy charged into or withdrawn from a battery, considering the time-varying nature in the renewable energy output. A salient aspect of our formulation is that it enables real-time updating of a joint predictive-prescriptive model where forecasts of energy outputs over the future horizon are used to update decisions. This scheme is enabled via FPCA which accounts for data heterogeneity, safeguards against model mis-specification via non-parametric predictions and features a linear decomposition which in turn enables efficient real-time updating. We show that our scheme is flexible to different optimization schemes; be it stochastic, robust or even a deterministic approach. Our technology is then tested on the California ISO data set [33]. This case study provided a proof-of-concept that highlights both the benefits and ease of implementation of our forward looking framework.

Our model can be extended in various directions. For instance, one may consider the battery degradation over time by providing a predictive model to update the capacity limits, much like how FPCA is predicting supply. In addition, planning decisions for optimal needed battery capacity is an important problem, in particular, with large penetration of volatile renewable energy in the electricity market. Such a problem might benefit from a non-myopic approach such as ours, especially since FPCA can hand both short and long term predictions as long as all historical and to be-predicted functions share the same domain. We hope to work on such challenges in the future.

#### References

- [1] M. You, E. Byon, J. J. Jin, and G. Lee, "When wind travels through turbines: A new statistical approach for characterizing heterogeneous wake effects in multi-turbine wind farms," *IISE Transactions*, vol. 49, no. 1, pp. 84–95, 2017.
- "State [2] L.M. Sixel, mandates for renewables is driving new projects," wind. solar power *Houston* Chronicle. 2019,from: https://www.houstonchronicle.com/business/energy/article/State-mandates-forrenewables-is-driving-new-13652699.php#photo-15932105.
- [3] S. Ahmed, A. Mahmood, A. Hasan, G. A. S. Sidhu, and M. F. U. Butt, "A comparative review of china, india and pakistan renewable energy sectors and sharing opportunities," *Renewable and Sustainable Energy Reviews*, vol. 57, pp. 216–225, 2016.
- [4] C. Clastres, T. H. Pham, F. Wurtz, and S. Bacha, "Ancillary services and optimal household energy management with photovoltaic production," *Energy*, vol. 35, no. 1, pp. 55–64, 2010.
- [5] T. Hesser and S. Succar, "Chapter 9-renewables integration through direct load control and demand response smart grid (pp. 209-233)," 2012.

- [6] California Independent System Operator, "California iso home page," 2019, from: http://www.caiso.com/Pages/default.aspx.
- [7] P. Denholm, M. O'Connell, G. Brinkman, and J. Jorgenson, "Overgeneration from solar energy in california. a field guide to the duck chart," National Renewable Energy Lab.(NREL), Golden, CO (United States), Tech. Rep., 2015.
- [8] California Independent System Operator, "Impacts of renewable energy on grid operations," 2017, from: https://www.caiso.com/Documents/CurtailmentFastFacts.pdf.
- [9] L. Hirth, "The market value of variable renewables: The effect of solar wind power variability on their relative price," *Energy economics*, vol. 38, pp. 218–236, 2013.
- [10] F. Giraud and Z. M. Salameh, "Steady-state performance of a grid-connected rooftop hybrid wind-photovoltaic power system with battery storage," *IEEE Power Engineering Review*, vol. 21, no. 2, pp. 54–54, 2001.
- [11] F. Lambert, "Tesla's massive powerpack battery in australia cost \$66 million and already made up to \$17 million," *Electrek*, 2018, from: https://electrek.co/2018/09/24/tesla-powerpack-battery-australia-cost-revenue/.
- [12] K. M. Chandy, S. H. Low, U. Topcu, and H. Xu, "A simple optimal power flow model with energy storage," in 49th IEEE Conference on Decision and Control (CDC). IEEE, 2010, pp. 1051–1057.
- [13] A. Parisio and L. Glielmo, "A mixed integer linear formulation for microgrid economic scheduling," in 2011 IEEE International Conference on Smart Grid Communications (SmartGridComm). IEEE, 2011, pp. 505–510.
- [14] Y. Wang, X. Lin, and M. Pedram, "Adaptive control for energy storage systems in households with photovoltaic modules," *IEEE Transactions on Smart Grid*, vol. 5, no. 2, pp. 992–1001, 2014.
- [15] M. He, S. Murugesan, and J. Zhang, "A multi-timescale scheduling approach for stochastic reliability in smart grids with wind generation and opportunistic demand," *IEEE Transactions on Smart Grid*, vol. 4, no. 1, pp. 521–529, 2013.
- [16] M. J. Neely, "Stochastic network optimization with application to communication and queueing systems," *Synthesis Lectures on Communication Networks*, vol. 3, no. 1, pp. 1–211, 2010.
- [17] Y. Guo, Y. Gong, Y. Fang, P. P. Khargonekar, and X. Geng, "Energy and network aware workload management for sustainable data centers with thermal storage," *IEEE Transactions on Parallel and Distributed Systems*, vol. 25, no. 8, pp. 2030–2042, 2013.
- [18] T. Li and M. Dong, "Online control for energy storage management with renewable energy integration," in 2013 IEEE International Conference on Acoustics, Speech and Signal Processing. IEEE, 2013, pp. 5248–5252.

- [19] S. Xia, Z. Ding, T. Du, D. Zhang, M. Shahidehpour, and T. Ding, "Multitime scale coordinated scheduling for the combined system of wind power, photovoltaic, thermal generator, hydro pumped storage, and batteries," *IEEE Transactions on Industry Applications*, vol. 56, no. 3, pp. 2227–2237, 2020.
- [20] N. Li, C. Uckun, E. M. Constantinescu, J. R. Birge, K. W. Hedman, and A. Botterud, "Flexible operation of batteries in power system scheduling with renewable energy," *IEEE Transactions on Sustainable Energy*, vol. 7, no. 2, pp. 685–696, 2015.
- [21] C. Uçkun, A. Botterud, and J. R. Birge, "An improved stochastic unit commitment formulation to accommodate wind uncertainty," *IEEE Transactions on Power Systems*, vol. 31, no. 4, pp. 2507–2517, 2015.
- [22] W. Su, J. Wang, and J. Roh, "Stochastic energy scheduling in microgrids with intermittent renewable energy resources," *IEEE Transactions on Smart Grid*, vol. 5, no. 4, pp. 1876–1883, 2014.
- [23] A. H. Habib, V. R. Disfani, J. Kleissl, and R. A. de Callafon, "Market-driven energy storage planning for microgrids with renewable energy systems using stochastic programming," *IFAC-PapersOnLine*, vol. 50, no. 1, pp. 183–188, 2017.
- [24] E. Du, N. Zhang, B.-M. Hodge, Q. Wang, Z. Lu, C. Kang, B. Kroposki, and Q. Xia, "Operation of a high renewable penetrated power system with csp plants: A look-ahead stochastic unit commitment model," *IEEE Transactions on Power Systems*, vol. 34, no. 1, pp. 140–151, 2018.
- [25] H. Shuai, J. Fang, X. Ai, J. Wen, and H. He, "Optimal real-time operation strategy for microgrid: An adp-based stochastic nonlinear optimization approach," *IEEE Transactions on Sustainable Energy*, vol. 10, no. 2, pp. 931–942, 2018.
- [26] N. G. Cobos, J. M. Arroyo, N. Alguacil, and J. Wang, "Robust energy and reserve scheduling considering bulk energy storage units and wind uncertainty," *IEEE Transactions on Power Systems*, vol. 33, no. 5, pp. 5206–5216, 2018.
- [27] J. H. Kim and W. B. Powell, "Optimal energy commitments with storage and intermittent supply," *Operations research*, vol. 59, no. 6, pp. 1347–1360, 2011.
- [28] D. F. Salas and W. B. Powell, "Benchmarking a scalable approximate dynamic programming algorithm for stochastic control of grid-level energy storage," *INFORMS Journal on Computing*, vol. 30, no. 1, pp. 106–123, 2017.
- [29] S. Kwon, Y. Xu, and N. Gautam, "Meeting inelastic demand in systems with storage and renewable sources," *IEEE Transactions on Smart Grid*, vol. 8, no. 4, pp. 1619–1629, 2015.
- [30] A. V. Savkin, M. Khalid, and V. G. Agelidis, "A constrained monotonic charging/discharging strategy for optimal capacity of battery energy storage supporting wind farms," *IEEE Transactions on Sustainable Energy*, vol. 7, no. 3, pp. 1224–1231, 2016.

- [31] T. Bjork, Arbitrage Theory in Continuous Time. Oxford University Press, 2009.
- [32] F. Yao, H.-G. Müller, and J.-L. Wang, "Functional data analysis for sparse longitudinal data," *Journal of the American Statistical Association*, vol. 100, no. 470, pp. 577–590, 2005.
- [33] I. S. O. California, "Production and curtailments data," 2019, from: http://www.caiso.com/informed/Pages/ManagingOversupply.aspx.
- [34] C. I. S. Operator, "2019 first quarter report on market issues and performance," 2019, from: http://www.caiso.com/market/Pages/MarketMonitoring.
- [35] H. Hullait, D. S. Leslie, N. G. Pavlidis, and S. King, "Robust function-on-function regression," *Technometrics*, pp. 1–14, 2020.

## A Robust Approach

$$\min \max_{i} \left\{ \sum_{t=0}^{T-1} \rho^{t} \cdot \left[ c_{salvage}(t) \cdot \left( O_{excess}^{(i)}(t) + O_{B}^{(i)}(t) \right) + c_{spot}(t) \cdot \left( O_{shortage}^{(i)}(t) + U_{B}^{(i)}(t) \right) \right] + \rho^{T} \Phi(B_{i}(T)) \right\},$$
(25)

In LP formulation,

$$\min F$$
,

s.t. 
$$F \ge \sum_{t=0}^{T-1} \rho^t \cdot \left[ c_{salvage}(t) \cdot (O_{excess}^{(i)}(t) + O_B^{(i)}(t)) + c_{spot}(t) \cdot (O_{shortage}^{(i)}(t) + U_B^{(i)}(t)) \right] + \rho^T \Phi(B_i(T))$$
 (26)

Other constraints remain the same as scenario-based approach (22).

#### B FPCA considerations

Functional regression methods are often vulnerable in outliers [35]. Our FPCA model can also exhibit sensitivity when data contains outliers. For example, the Bayesian updating scheme above may lead to inaccurate predictions if recent observations stray away from the previously observed trends. To deal with this issue, we adopt a simple strategy. First, we smoothen the curves to alleviate local fluctuations. We used a Gaussian kernel smoother in our numerical study, but other smoothers can be employed. Next, if an observation lies outside our 3-sigma prediction interval, we ignore it and wait until the next observation to update our model. If h consecutive recent observations are out of the 3-sigma limits we relax this restriction.

## C Results

Table 3: Non-myopic approach: regret ratio with varying spot prices and discounting factor ( $\rho=0.999$ )

Non-myopic	Expectation	Scenario	Scenario	Scenario
$\_\_approach$		2	5	10
Apr 17, 2018	9.35%	10.62%	9.34%	7.93%
Apr 18, 2018	1.76%	1.75%	1.39%	1.26%
Apr 19, 2018	15.01%	16.79%	13.77%	12.98%
Apr 20, 2018	12.16%	13.12%	10.80%	10.38%
Apr 23, 2018	3.65%	4.08%	3.42%	3.37%
Apr 24, 2018	6.01%	6.57%	5.21%	5.11%
Apr 25, 2018	7.11%	8.30%	6.22%	6.17%
Apr 26, 2018	6.22%	9.88%	7.15%	5.31%
Apr 27, 2018	6.45%	10.25%	7.60%	5.92%
Apr 30, 2018	4.38%	7.06%	5.67%	4.93%
Average	7.21%	8.84%	7.06%	6.34%

Table 4: Myopic approach: regret ratio with varying spot prices and discounting factor ( $\rho=0.999$ )

$\phantom{aaaaaaaaaaaaaaaaaaaaaaaaaaaaaaaaaaa$	Expectation	Scenario	Scenario	Scenario
approach		2	5	10
Apr 17, 2018	10.46%	10.36%	10.36%	10.36%
Apr 18, 2018	9.70%	10.03%	9.77%	9.70%
Apr 19, 2018	14.53%	14.81%	14.59%	14.56%
Apr 20, 2018	18.34%	18.61%	18.42%	18.52%
Apr 23, 2018	9.47%	9.56%	9.48%	9.53%
Apr 24, 2018	13.13%	12.94%	12.90%	13.01%
Apr 25, 2018	10.56%	10.56%	10.53%	10.53%
Apr 26, 2018	11.08%	11.37%	11.17%	11.18%
Apr 27, 2018	10.11%	10.34%	10.02%	10.20%
Apr 30, 2018	10.69%	10.74%	10.77%	10.73%
Average	11.81%	11.93%	11.82%	11.83%

Table 5: Non-myopic approach: regret ratio with varying spot prices and discounting factor ( $\rho=0.999$ )

$Non ext{-}myopic$	Expectation	Robust	Robust	Robust
approach		2	5	10
Apr 17, 2018	9.35%	10.48%	10.49%	10.45%
Apr 18, 2018	1.76%	10.05%	10.05%	10.24%
Apr 19, 2018	15.01%	14.61%	14.82%	14.81%
Apr 20, 2018	12.16%	18.64%	18.55%	18.82%
Apr 23, 2018	3.65%	9.53%	9.73%	9.71%
Apr 24, 2018	6.01%	13.10%	13.54%	13.51%
Apr 25, 2018	7.11%	10.27%	10.65%	10.77%
Apr 26, 2018	6.22%	11.34%	11.65%	11.74%
Apr 27, 2018	6.45%	10.33%	10.53%	10.56%
Apr 30, 2018	4.38%	10.81%	10.85%	10.91%
Average	7.21%	11.95%	12.09%	12.15%

Table 6: Myopic approach: regret ratio with varying spot prices and discounting factor ( $\rho=0.999$ )

$\overline{Myopic}$	Expectation	Robust	Robust	Robust
approach		2	5	10
Apr 17, 2018	10.46%	10.42%	10.57%	10.53%
Apr 18, 2018	9.70%	9.86%	9.76%	9.82%
Apr 19, 2018	14.53%	14.48%	14.40%	14.37%
Apr 20, 2018	18.34%	18.69%	18.61%	18.57%
Apr 23, 2018	9.47%	9.45%	9.48%	9.48%
Apr 24, 2018	13.13%	12.84%	12.88%	12.91%
Apr 25, 2018	10.56%	10.54%	10.50%	10.56%
Apr 26, 2018	11.08%	11.06%	11.07%	11.07%
Apr 27, 2018	10.11%	10.19%	10.18%	10.16%
Apr 30, 2018	10.69%	10.68%	10.72%	10.69%
Average	11.81%	11.82%	11.82%	11.82%

Table 7: Average Computational time for all approaches

-			
Proposed Methods	Running time (sec)		
	Myopic	Non-Myopic	
Expectation	0.001	145.21	
Scenario 2	2.07	60.16	
Scenario 5	2.10	332.92	
Scenario 10	2.37	1676.10	
Robust 2	2.26	73.85	
Robust 5	2.42	428.36	
Robust 10	2.66	2199.4	